Current and optimal dimensions predictions for a porous micro-electrode

Tien Dung Le, Didier Lasseux

ChemElectroChem 2020, *7*, 3017 – 3027 doi.org/10.1002/celc.202000508

Current and Optimal Dimensions Predictions for a Porous Micro-Electrode

Tien D. Le[a] and Didier Lasseux*[b]

The expression of the current delivered by a cylindrical porous micro-electrode operating a single heterogeneous reaction and mass diffusion of the reagent is analytically derived in this work from a *complete solution* of the diffusion/reaction macroscopic problem. This solution is valid regardless of the aspect (thickness to inner radius) ratio. It encompasses the *hybrid solution* reported elsewhere, valid only when this ratio remains small compared to unity, and, consequently, the case of a planar electrode as well. The asymptotic form of the solution in this latter case is also provided. The complete solution is used to predict the optimal thickness of the electrode and its optimal inner radius (*i.e.* the supporting wire radius) corresponding to the best compromise between a minimum electrode volume and a maximum current per unit volume. This work hence provides a complete optimization procedure that can be used as predictive tools for the design of porous electrodes.

1. Introduction

The development of miniaturized electrodes has been the subject of intense interest for the past decade, in particular for bio-implantable electro-devices.[1] In order to reduce their size, micro- or nanoporous materials are particulary attractive due to their high specific surface area available for the heterogeneous redox reactions, hence producing a much larger current than a flat electrode of the same size.[2] An abundant literature has been dedicated to the study of these devices, both from theoretical and experimental points of view. Many different operating conditions can be envisaged for these electrodes[3–6], namely without any catalyst[7,8] or with an embedded enzyme to catalyze the redox reactions which may occur in the direct electron transfer[9] or mediated electron transfer mode.[10] A classical procedure to obtain a porous material relies on a Langmuir-Blodgett templating method related to self-assembly of particles. This is followed by electrodeposition of a conducting material. After dissolving the particles, a synthetic porous electrode composed of interconnected pores is obtained which porosity and internal architecture can be tuned.[2,11, 12]

The coupled process of transport and electrochemical reaction occurring during voltammetry experiments for porous electrodes has been modelled in both cases with or without catalysis.[13–15] Recently, a multiscale model for a porous electrode operating a single reaction was developed[7], providing a macroscopic model and a closure problem which solution allows determining the effective parameter (effective diffusion coefficient). Such a model was validated by comparing its predictions with 3D direct numerical simulations at the pore scale similar to those reported recently.[16] It was also successfully compared with experimental data. The advantage of such an approach is that the ensuing macroscale model, which contains the necessary information from the microscale, is much simpler to solve than the original one at the scale of the microstructure, avoiding cumbersome direct numerical simulations at this scale. Further, an optimization procedure, based on the macroscopic model to estimate the optimal thickness of cylindrical porous electrodes, has been investigated.[17] It was derived under the assumption that the electrode thickness is much smaller than its inner radius, although the diffusion layer thickness surrounding the electrode is not. This yielded the so-called *hybrid model*. However, such an assumption can fail in practice and it is hence of major interest to derive a prediction of the optimal thickness in the general case.

In the present work, an accurate *complete solution* of the upscaled model in its general form is proposed in order to predict the current delivered by a cylindrical electrode in the steady regime and to estimate its optimal thickness and optimal inner radius without any assumption on its microstructure and dimensions. This solution is expressed in terms of the Bessel's functions of the first and second kinds; it is valid whatever the thickness to inner radius ratio and is hence general.

Predictions of this model are compared to those obtained from the hybrid model in the case of a face-centered cubic, cubic and body-centered cubic structures of the porous material. Moreover, an analytical solution is also derived for planar electrodes which conveniently matches the complete solution for cylindrical electrodes in the limit of an extremely large radius compared to the thickness. Finally, the optimal radius of the supporting wire that leads to the minimum volume of the electrode is derived. This represents a very important result, leading to a complete optimization process of the macroscopic dimensions of the electrode.

The paper is organized as follows. In Section 2, the upscaled model for the coupled electrochemical reaction and transport in a porous micro-electrode is briefly recalled. A complete analytical solution of the macroscopic model for a cylindrical

[a] *Dr. T. D. Le*
I2M, UMR 5295, CNRS, Univ. Bordeaux, Esplanade des Arts et Métiers, 33405 Talence CEDEX, France - Université de Lorraine, CNRS, LEMTA, F-54000 Nancy, France
[b] *Dr. D. Lasseux*
I2M, UMR 5295, CNRS, Univ. Bordeaux, Esplanade des Arts et Métiers, 33405 Talence CEDEX, France
E-mail: didier.lasseux@u-bordeaux.fr

geometry is proposed in Section 3 without any restriction on the electrode dimensions. Such a solution is compared to that of the hybrid model developed in Ref. [17] to predict the optimal electrode thickness. In Section 4, an analytical solution of the macroscopic model and for the optimal thickness of a planar electrode is proposed. Section 5 is dedicated to the derivation of the optimal radius of the cylindrical wire supporting the electrode, which, along with its optimal thickness, provides a complete framework for its macroscopic optimization. Concluding remarks are drawn in Section 6.

2. Recall of the upscaled model

In this section, the upscaled model for a porous electrode operating a single reduction reaction, as proposed in previous works[7,17], is briefly recalled to further develop its solution. This model is derived from the pore-scale initial boundary value problem (IBVP) describing the coupled diffusion and heterogeneous reaction of the species of interest. Diffusion of this species, A, (of molar concentration c_A) dissolved in the solution saturating the electrode's pore space, denoted Ω_f, is governed by Fick's law.[18] It is beyond the scope of this article to provide the details for this governing law to apply here. The reader is referred to Ref. [19] for the assumptions and constraints that support it. At the pore solid/fluid interfaces, $\mathcal{I}_{sf}$, a single reaction reducing A is considered for which the electron transfer mechanism is described by the Butler-Volmer's relation[20] (see Figure 1).

The IBVP at the pore scale can be formulated as follows

$$\frac{\partial c_A}{\partial t} = \boldsymbol{\nabla}\cdot(\mathcal{D}_A\boldsymbol{\nabla}c_A) \qquad \text{in } \Omega_f \tag{1a}$$

$$\text{B.C.1} \quad -\mathbf{n}\cdot\mathcal{D}_A\boldsymbol{\nabla}c_A = k_0\alpha_A c_A \qquad \text{at } \mathcal{I}_{sf} \tag{1b}$$

$$\text{B.C.2} \quad c_A = \mathcal{G}_A(\mathbf{r},t) \qquad \mathbf{r}\in A_{fe},\ \forall\, t \tag{1c}$$

$$\text{I.C.} \quad c_A = \mathcal{F}_A(\mathbf{r}) \qquad \mathbf{r}\in\Omega_f,\ t=0 \tag{1d}$$

In these equations, $\mathcal{D}_A$ is the molecular diffusion coefficient of species A, $\mathbf{n}$ denotes the unit normal vector at $\mathcal{I}_{sf}$, pointing out of Ω_f, and k_0 is the standard rate constant of the reaction.

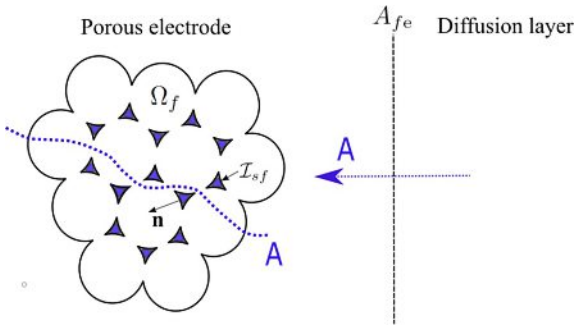

Figure 1. Pore-scale configuration.

Moreover, $\alpha_A = \exp\left(\frac{-\alpha n F(E-E^0)}{RT}\right)$ where α, n, E and E^0 are the electron transfer coefficient, the number of transferred electrons, the electrode potential and the standard potential respectively, F, R and T representing the Faraday's constant, ideal gas constant and temperature. In this work, T is assumed to be constant and the conduction of electrons in the solid phase is supposed to be extremely fast so that the potential in this phase can be readily considered as uniform. It should be noted that in the boundary condition B.C.2, $A_{fe}=\Omega_f\cap\Omega_e$ is the entrance and/or exit boundaries of the fluid phase, Ω_f, from/into the diffusion layer surrounding the electrode, denoted Ω_e.

The above pore-scale IBVP can be upscaled using the volume averaging method[21] to obtain a model at the macroscopic scale. To do so, a separation of length-scales is assumed between the characteristic pore length-scale, ℓ_p, and the characteristic macroscopic length scale, L, of the system. In addition, it is assumed that an intermediate scale r_0 can be exhibited satisfying $\ell_p \ll r_0 \ll L$ such that an averaging domain, V, of measure V and size r_0 can be used to average the pore-scale IBVP. The domain V is usually chosen so as to contain all the necessary microstructural information in order to be a representative elementary volume (REV) of the porous medium and of the physical process at play. In this way, the macroscopic model is expressed in terms of the intrinsic average concentration of species A, denoted $\langle c_A\rangle^f$. It is defined in V in which the fluid phase occupies a domain V_f, of measure V_f, as

$$\langle c_A\rangle^f = \frac{1}{V_f}\int_{\mathrm{V}_f(\mathbf{x})} c_A\, dV \tag{2}$$

The averaging procedure is then carried out in three main steps. The averaging operator of Eq. 2 is first applied to the pore-scale IBVP, and in order to interchange time and space derivations with integration, the general transport theorem[22] and the averaging theorem[23] are employed. When the porous medium is rigid and homogeneous, they can be respectively expressed as

$$\left\langle\frac{\partial\psi}{\partial t}\right\rangle^f = \frac{\partial\langle\psi\rangle^f}{\partial t} \tag{3a}$$

$$\langle\nabla\psi\rangle^f = \nabla\langle\psi\rangle^f + \frac{1}{V_f}\int_{\mathcal{A}_{sf}}\mathbf{n}\psi\, dA \tag{3b}$$

In the latter, $\mathcal{A}_{sf}$, of measure A_{sf}, represents the portion of $\mathcal{I}_{sf}$ contained in V. In a second step, the physical variables ψ (here $\psi = c_A$) are spatially decomposed under the form $\psi = \langle\psi\rangle^f + \tilde{\psi}$,[24] $\tilde{\psi}$ representing the spatial fluctuations of ψ with respect to its average $\langle\psi\rangle^f$. This decomposition is introduced in the averaged equations which can be usually simplified on the basis of the scale hierarchy. This yields an unclosed model in which both $\langle\psi\rangle^f$ and $\tilde{\psi}$ are present. In a third step, the (initial) boundary value problem for $\tilde{\psi}$ is derived and this is obtained by subtracting the unclosed macroscopic equations from their pore-scale analogues. The equations for $\tilde{\psi}$

are then simplified on the basis of the length scale constraints. These constraints further allow obtaining a formal solution expressed in terms of *closure variables* by making the problem on $\tilde{\psi}$ periodic over a periodic unit cell, at least as large as the REV. For simplicity, this periodic unit cell is identified as the REV in the remainder of this work. The formal solution for $\tilde{\psi}$ is introduced in the unclosed macroscopic equations, on the one hand, and in the problem for $\tilde{\psi}$, on the other hand, yielding the closed macroscopic model and the *closure problem(s)* for the closure variables, respectively. The closed model involves effective coefficients that are determined from the solution of the closure problem(s).

When the procedure described above is applied to the IBVP given in Eqs. 1, the following macroscopic mass conservation equation is obtained[7,17]

$$\varepsilon_f \frac{\partial \langle c_A \rangle^f}{\partial t} = \boldsymbol{\nabla} \cdot \left(\varepsilon_f \mathbf{D}_{eff} \cdot \boldsymbol{\nabla} \langle c_A \rangle^f \right) - k_0 \alpha_A a_v \langle c_A \rangle^f \qquad \text{in } \Omega \tag{4}$$

Here, Ω denotes the macroscopic domain occupied by the electrode whereas ε_f and a_v are the porosity and specific area, respectively defined by

$$\varepsilon_f = \frac{V_f}{V};\ a_v = \frac{A_{sf}}{V} \tag{5}$$

In addition, in Eq. 4, $\mathbf{D}_{eff}$ is the effective diffusion tensor which is computed from the solution of an intrinsic closure problem in a periodic REV (see Eqs. (16) reported in a previous work.[7]) An example of a REV, of size $\ell_R \equiv r_0$, is depicted in Figure 2 for a FCC structure constitutive of a porous electrode.

It should be noted that the second term on the right hand side of Eq. 4 originates from the heterogeneous reduction reaction of species *A* indicated in the pore-scale boundary condition in Eq. 1b that is now reflected in the macroscopic mass conservation equation. The current delivered by the electrode can then be expressed from the average concentration as[7]

$$I = -nk_0 F \alpha_A a_v \int_\Omega \langle c_A \rangle^f \mathrm{d}V \tag{6}$$

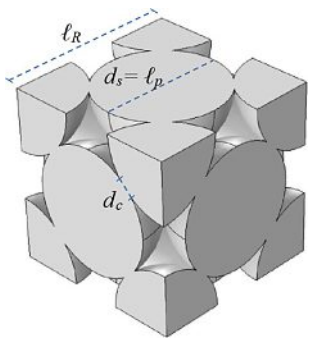

Figure 2. Unit cell of a FCC structure with the characteristic dimensions. The gray area corresponds to the fluid domain while the solid phase is not represented. Spherical pores are connected through windows of diameter d_c.

To obtain the solution on $\langle c_A \rangle^f$ in Ω, macroscopic boundary and initial conditions corresponding to the pore-scale analogues in Eqs. 1c and 1d must be specified. In practice, the electrode is immersed in the fluid saturating the pores. The mass transfer of species *A* in the surrounding bulk fluid, which is assumed to obey Fick's second law (Eq. 1a), gives rise to a diffusion layer, of thickness L_N, next to the fluid-electrode boundary. The concentration at the outer edge of this boundary layer remains constant over time and is denoted c_A^0 which is assumed to be the uniform concentration value in the whole system at $t = 0$. At the boundary between the electrode and the diffusion layer, continuity of both the concentration and the flux can be reasonably assumed as was investigated earlier.[7] A resistance to mass transfer may be considered at the fluid-electrode boundary. However, this mechanism would contribute to hinder the penetration of species *A* inside the electrode and would hence lead to predict an optimal thickness smaller than that in the absence of this mechanism. In the following the existence of mass transfer resistance is ignored with the idea that this leads to the maximum expected value of the optimal electrode thickness. Moreover, in order to determine this optimal thickness, the stationary regime is to be considered for which the penetration depth of the diffusion/reaction front has settled down inside the electrode.

The solution of the coupled diffusion-reaction macroscopic equation 4, considering the diffusion layer in the bulk fluid next to Ω, was proposed for a cylindrical electrode in the stationary regime.[17] However, this solution was restricted to the case where the thickness of the electrode remains small compared to its inner radius, although this assumption may not apply to the outer boundary layer thickness. This led to a so-called hybrid model. In practice, the electrode can be thick enough for this assumption to fail and it is hence of major importance to reconsider the problem in a more general case by deriving a solution referred to as the complete solution (or *Bessel's solution*). This is the purpose of the following section.

3. Cylindrical electrode

The cylindrical electrode under consideration is made of a porous material deposited on a conducting cylindrical wire of radius R_1. Its thickness is L_e and its external radius $R_2 = R_1 + L_e$. The diffusion layer outside the electrode is supposed to have an external radius $R_3 = R_2 + L_N$. A schematic cross section of the configuration, with the normalized characteristic radial dimensions denoted with the superscript *, is depicted in Figure 3. The reference dimension used to normalize the radial coordinate is the characteristic size, ℓ_R, of the periodic unit cell (the REV) of the porous medium. The wire center is positioned at $r^* = 0$.

Using the initial concentration c_A^0, that is supposed to be uniform in the whole system at $t = 0$, as the reference concentration, and assuming that steady state is reached, the macroscale problem takes the following form

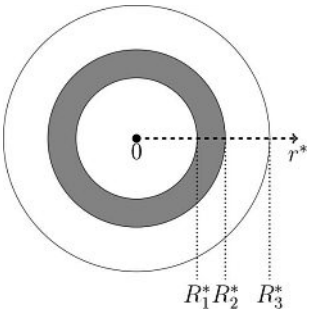

Figure 3. Cross section of a cylindrical electrode of external dimensionless radius $R_2{}^*$ made of a porous material (gray area) deposited on a cylindrical wire of dimensionless radius $R_1{}^*$ and surrounded by the diffusion layer which external dimensionless radius is $R_3{}^*$.

$$r^{*2}\frac{\mathrm{d}^2\langle c_A{}^*\rangle^f}{\mathrm{d}r^{*2}} + r^*\frac{\mathrm{d}\langle c_A{}^*\rangle^f}{\mathrm{d}r^*} = \varphi^2 r^{*2}\langle c_A{}^*\rangle^f \qquad R_1{}^* \le r^* \le R_2{}^* \qquad (7a)$$

$$\frac{\mathrm{d}}{\mathrm{d}r^*}\left(r^*\frac{\mathrm{d}c_A{}^*}{\mathrm{d}r^*}\right) = 0 \qquad R_2{}^* \le r^* \le R_3{}^* \qquad (7b)$$

$$\text{B.C.1}: \mathrm{D}_{eff}{}^*\frac{\mathrm{d}\langle c_A{}^*\rangle^f}{\mathrm{d}r^*} = \frac{\mathrm{d}c_A{}^*}{\mathrm{d}r^*} \qquad r^* = R_2{}^* \qquad (7c)$$

$$\text{B.C.2}: \langle c_A{}^*\rangle^f = c_A{}^* \qquad r^* = R_2{}^* \qquad (7d)$$

$$\text{B.C.3}: \frac{\mathrm{d}\langle c_A{}^*\rangle^f}{\mathrm{d}r^*} = 0 \qquad r^* = R_1{}^* \qquad (7e)$$

$$\text{B.C.4}: c_A{}^* = 1 \qquad r^* = R_3{}^* \qquad (7f)$$

In B.C.1 and B.C.2, continuity of both the flux and the concentration is assumed at the porous electrode-diffusion layer interface ($r^* = R_2{}^*$). At the electrode-wire interface, $r^* = R_1{}^*$, a zero flux is considered whereas a Dirichlet boundary condition is used at the external boundary of the diffusion layer ($r^* = R_3{}^*$) where the initial concentration, c_A^0, is imposed. In Eq. 7c, $\mathrm{D}_{eff}{}^* = \varepsilon_f \mathrm{D}_{eff}/\mathcal{D}_A$ ($\mathbf{D}_{eff} = \mathrm{D}_{eff}\mathbf{I}$ for an isotropic structure) and in Eq. 7a, φ is the Thiele modulus defined as

$$\varphi = \sqrt{\frac{Ki\, a_v{}^*}{D_{eff}{}^*}} \qquad (8)$$

where *Ki* is the kinetic number

$$Ki = \frac{k_0\alpha_A\ell_R}{\mathcal{D}_A} \qquad (9)$$

3.1. Hybrid model

When $L_e{}^*/R_1{}^* \ll 1$, Eq. 7a can be simplified to the following form

$$\frac{\mathrm{d}^2\langle c_A{}^*\rangle^f}{\mathrm{d}r^{*2}} - \varphi^2\langle c_A{}^*\rangle^f = 0, \qquad R_1{}^* \le r^* \le R_2{}^* \qquad (10)$$

In the absence of any other assumption (in particular if $L_e{}^* + L_N{}^*$ is not assumed to be exceedingly small compared to $R_1{}^*$), Eqs. 7b to 7f remain unchanged. This yields the hybrid model which solution is given by[17]

$$\langle c_A{}^*\rangle^f = a_1\cosh(\varphi(r^* - R_1{}^*)) \qquad R_1{}^* \le r^* \le R_2{}^* \qquad (11a)$$

$$c_A{}^* = b_1\ln r^* + c_1 \qquad R_2{}^* \le r^* \le R_3{}^* \qquad (11b)$$

with

$$a_1 = (\mathrm{D}_{eff}{}^*\varphi\sinh(\varphi L_e{}^*)R_2{}^*\ln(R_3{}^*/R_2{}^*) + \cosh(\varphi L_e{}^*))^{-1} \qquad (12a)$$

$$b_1 = \left(\frac{\coth(\varphi L_e{}^*)}{\mathrm{D}_{eff}{}^*R_2{}^*\varphi} + \ln(R_3{}^*/R_2{}^*)\right)^{-1} \qquad (12b)$$

$$c_1 = 1 - b_1\ln(R_3{}^*) \qquad (12c)$$

Moreover, the current per unit volume can be expressed as

$$\frac{I}{V_e} = -\frac{nFk_0\alpha_A a_v c_A^0}{\varphi L_e{}^*[\coth(\varphi L_e{}^*) + \mathrm{D}_{eff}{}^*\varphi R_2{}^*\ln(R_3{}^*/R_2{}^*)]} \qquad (13)$$

where V_e is the volume of the electrode immersed in the reactive solution, *i.e.*, the active electrode volume.

3.2. Complete solution

At this point, no special hypothesis is made on the electrode dimensions and Eqs. 7 are kept as such. The solution of Eq. 7a is given by a linear combination of the modified zeroth order Bessel's functions of the first and second kinds, I_0 and K_0, as[25]

$$\langle c_A{}^*\rangle^f = A_1 I_0(\varphi r^*) + B_1 K_0(\varphi r^*), \qquad R_1{}^* \le r^* \le R_2{}^* \qquad (14)$$

The coefficients A_1 and B_1 can be determined by making use of the boundary conditions 7c, 7d, 7e and 7f. When this conditions are used, one obtains

$$A_1 = -\frac{K_1(\varphi R_1{}^*)}{I_1(\varphi R_1{}^*)}B_1 \qquad (15a)$$

$$B_1 = \left[-\frac{K_1(\varphi R_1{}^*)}{I_1(\varphi R_1{}^*)}I_0(\varphi R_2{}^*) + K_0(\varphi R_2{}^*) + \mathrm{D}_{eff}{}^*\varphi R_2{}^*\ln\frac{R_3{}^*}{R_2{}^*}\left(-\frac{K_1(\varphi R_1{}^*)}{I_1(\varphi R_1{}^*)}I_1(\varphi R_2{}^*) - K_1(\varphi R_2{}^*)\right)\right]^{-1} \qquad (15b)$$

where I_1 and K_1 are the first order modified Bessel's functions of the first and second kinds, respectively.

In the external diffusion layer, the concentration is given by

$$c_A^* = A_2 \ln r^* + B_2, \qquad R_2^* \le r^* \le R_3^* \tag{16}$$

with

$$A_2 = \frac{1}{\ln(R_2^*/R_3^*)}\left(A_1 I_0(\varphi R_2^*) + B_1 K_0(\varphi R_2^*) - 1\right) \tag{17a}$$

$$B_2 = 1 - A_2 \ln R_3^* \tag{17b}$$

When the solution given in Eq. 14 is introduced in Eq. 6, the current per unit active electrode volume, V_e, takes the following expression

$$\begin{aligned}\frac{I}{V_e} &= -\frac{C}{R_2^{*2} - R_1^{*2}} \int_{R_1^*}^{R_2^*} [A_1 I_0(\varphi r^*) + B_1 K_0(\varphi r^*)] r^* \mathrm{d}r^* \\ &= -\frac{C}{R_2^{*2} - R_1^{*2}} (A_1 F_1 + B_1 F_2)\end{aligned} \tag{18}$$

with C, F_1 and F_2 respectively given by

$$C = 2nk_0 F a_v \alpha_A c_A^0 \tag{19a}$$

$$F_1 = \int_{R_1^*}^{R_2^*} I_0(\varphi r^*) r^* \mathrm{d}r^* = \frac{1}{\varphi}(R_2^* I_1(\varphi R_2^*) - R_1^* I_1(\varphi R_1^*)) \tag{19b}$$

$$\begin{aligned}F_2 &= \int_{R_1^*}^{R_2^*} K_0(\varphi r^*) r^* \mathrm{d}r^* = \\ &\frac{1}{\varphi}(R_1^* K_1(\varphi R_1^*) - R_2^* K_1(\varphi R_2^*))\end{aligned} \tag{19c}$$

In the following, numerical evaluation of the above solution on the current versus the scanning potential is compared to that of the hybrid model. The parameters used to compute these solutions are given in Table 1. They correspond to those used for the validation of the macroscopic model with direct numerical simulations of the microscale model and experimental data.[7,17] The electrochemical reaction considered here is typically the reduction of H_2O_2 to H_2O. Moreover, the face-centered cubic (FCC) structure is assumed as the periodic REV of the porous medium constitutive of the electrode (see Figure 2). This structure is uniquely defined by the sphere diameter, $d_s \equiv \ell_p$, and the pore connection window size, d_c.[7] The REV of the FCC structure corresponds to 4 half-layers (HL) of spherical pores.

The current versus the potential obtained from both the hybrid model and Bessel's solution is represented in Figure 4 (a) for three different electrodes made of 5HL, 15HL and 30HL of pores. As can be observed from this figure, the two solutions are almost identical when the potential is sufficiently large, although the hybrid model tends to underestimate the magnitude of the current. The discrepancy between the two models becomes significant below a threshold value of the potential which increases with the electrode thickness. This is made clear in Figure 4 (b) representing the absolute value of the relative error between the two models (the Bessel's solution is taken as the reference) showing that this relative error can reach about 12 % for the thickest electrode under consideration when the potential is close to 0 *V*.

Table 1. Parameters used for the solutions of the hybrid and complete models.

Parameter[7,17]	Symbol	Value	Unit
Ideal gas constant	R	8.314	$\mathrm{J\,mol^{-1}K^{-1}}$
Faraday's constant	F	96485	$\mathrm{C\,mol^{-1}}$
Number of electron transferred	n	2	–
Electron transfer coefficient	α	0.482	–
Standard rate constant	k_0	1.7×10^{-17}	$\mathrm{cm\,s^{-1}}$
Standard potential vs. $E^0_{Ag/AgCl}$	E_0	1.56	V
Temperature	T	298	K
Bulk concentration	c_A^0	10	$\mathrm{mol\,m^{-3}}$
Diffusion coefficient	$\mathcal{D}_A$	10^{-9}	$\mathrm{m^2s^{-1}}$
Spherical pore diameter	$d_s = \ell_p$	1.17	μm
Pore connection window size	d_c	$0.15d_s$	m
Size of the periodic unit cell	ℓ_R	1.64	μm
Porosity	ε_f	0.763	–
Specific surface area	a_v	3.567×10^6	$\mathrm{m^{-1}}$
Normalized effective coefficient	$D_{eff}{}^*$	0.364	–
Wire radius	R_1	25	μm
Diffusion layer thickness	L_N	100	μm

Numerical simulations on other microstructures, namely cubic (C) and body-centered cubic (BCC) which unit cells are represented in Figure 5, are also carried out using the parameters given in Table 1. The resulting values of ε, a_v, $D_{eff}{}^*$ and ℓ_R are reported in Table 2. In Figure 6, the current versus the scanning potential obtained for different electrode thicknesses computed with the complete solution and the hybrid model are represented for the C (Figure 6 (a)) and BCC (Figure 6 (b)) structures. As already observed for the FCC structure, a significant difference between the two models exists in particular for a thick electrode, and this is a general feature for any microstructure. Again, the hybrid model accuracy fails

Table 2. Properties of C and BCC structures used in the simulations.

Parameter[7]	Symbol	Value	Unit
	C		
Porosity	ε_f	0.541	–
Specific surface area	a_v	2.68×10^6	$\mathrm{m^{-1}}$
Normalized effective diffusion coefficient	$D_{eff}{}^*$	0.142	–
Size of the periodic unit cell	ℓ_R	1.16	μm
	BCC		
Porosity	ε_f	0.703	–
Specific surface area	a_v	3.44×10^6	$\mathrm{m^{-1}}$
Normalized effective diffusion coefficient	$D_{eff}{}^*$	0.236	–
Size of the periodic unit cell	ℓ_R	1.34	μm

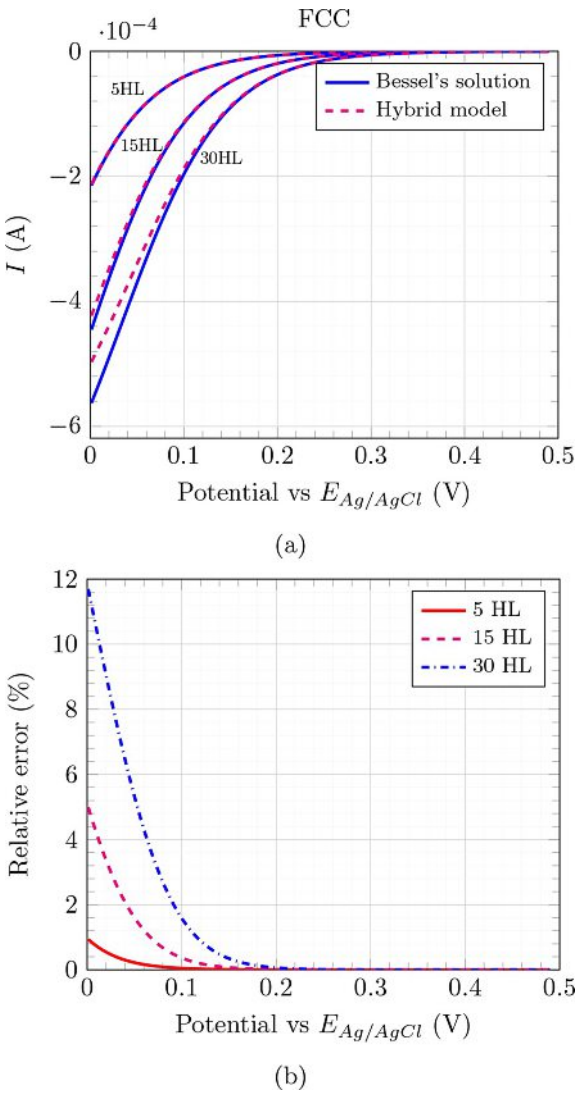

Figure 4. (a) Current versus the scanning potential obtained from the hybrid model and Bessel's solution for the 5HL, 15HL and 30 HL electrodes. (b) Absolute value of the relative error between the two solutions taking the Bessel's solution as the reference.

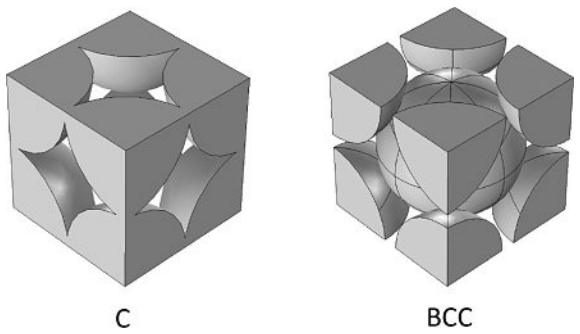

Figure 5. Unit cell of the C and BCC structures.

when the thickness to inner radius ratio is not small enough compared to 1.

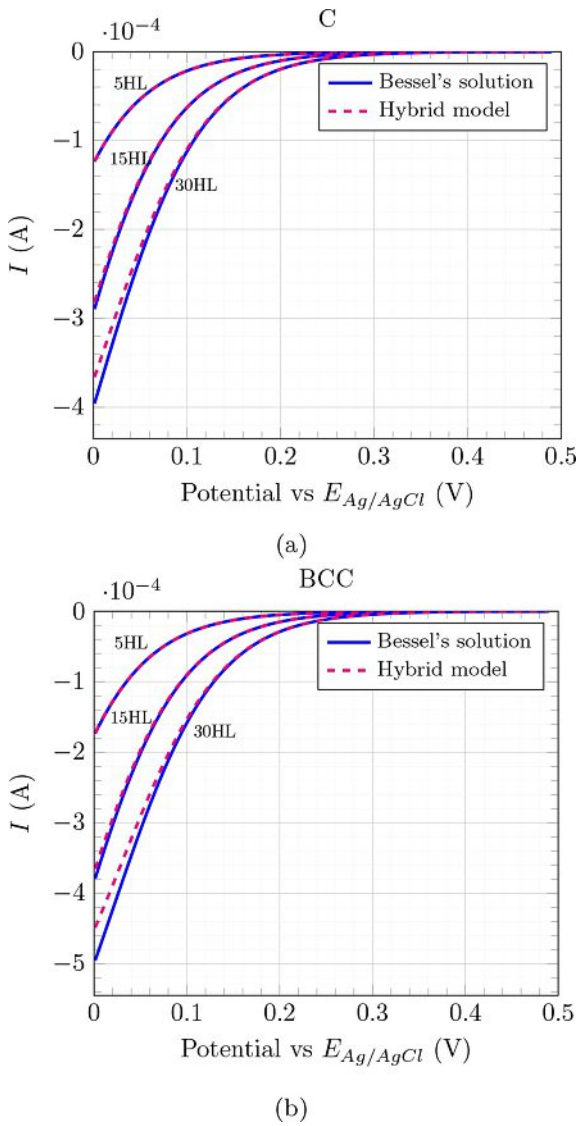

Figure 6. Current versus the scanning potential obtained from the hybrid model and Bessel's solution for the 5HL, 15HL and 30 HL electrodes: (a) cubic structure (C) (b) body-centered cubic structure (BCC).

The analysis can now be focused on the optimal electrode thickness using the same approach as the one recently investigated.[17] To begin with, it is instructive to illustrate the electrode efficiency with the reagent concentration profile. In Figure 7, $\langle c_A^* \rangle^f$ obtained from Eq. 14 with $L_e^* = 30$ and parameters of Table 1 is represented within the electrode ($R_1^* < r^* < R_2^*$) for $Ki = 10^{-4}$ and $Ki = 10^{-3}$. This figure clearly shows that the penetration depth of the concentration front inside the electrode decreases as the kinetic number increases, *i.e.* when reaction becomes more significant so that species *A* is consumed in the vicinity of the electrode/diffusion layer interface. As a result, a large part of the electrode (about half of it in Figure 7 for $Ki = 10^{-3}$), in the region far enough from this interface, does not contribute much to the current production. This observation is an evidence that an optimal thickness can be determined and this is carried out as follows.

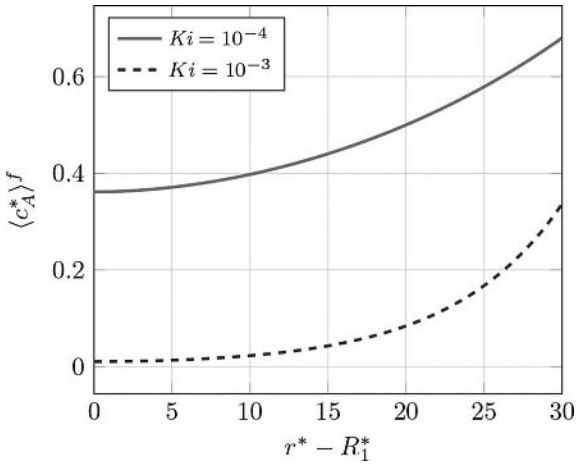

Figure 7. Normalized concentration profile of species *A* in the electrode for two values of the kinetic number. The dimensionless electrode thickness is $L_e^* = 30$ the other parameters being those in Table 1.

The current per unit volume expressed in Eq. 18 decreases with the electrode thickness, L_e^*, in two characteristic regimes (see Figure 8): a rapid decrease at small electrode thicknesses followed by a slow convergence to zero at very large values of L_e^*. This suggests defining the optimal thickness, L_e^{*op}, as the crossover between these two regimes. Practically, this value is obtained at the intersecting point of the tangent to $|I/V_e|$ at L_e^{*0} with $|I/V_e| = 0$. The value of L_e^{*0} should be taken as the minimum thickness that is experimentally achievable, *i.e.*, $L_e^{*0} \geq 1$. The value of L_e^{*op} can hence be obtained from the following expression

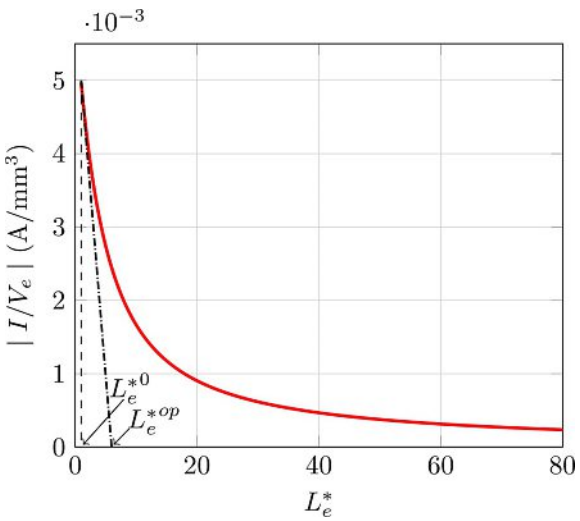

Figure 8. Variation of the current per unit volume, $|I/V_e|$, obtained from Eq. 18 versus the electrode's dimensionless thickness, L_e^*, in the case of a FCC microstructure for $Ki = 10^{-3}$ and $L_N = 100\ \mu$m. The other parameters used to compute the current per unit volume are provided in Table 1. The optimal thickness, L_e^{*op} is obtained from the intersection of the tangent to this graph at $L_e^* = L_e^{*0}$ with the axis $|I/V_e| = 0$. See text for the details.

$$L_e^{*op} = -\frac{|I/V_e|_{L_e^{*0}}}{\left.\frac{\partial |I/V_e|}{\partial L_e^*}\right|_{L_e^{*0}}} + L_e^{*0} \tag{20}$$

The derivative of the current per unit volume with respect to L_e^* involved in this last relationship can be determined analytically from Eq. 18. It is given by

$$\frac{\partial(|I/V_e|)}{\partial L_e^*} = \frac{2R_2^*}{R_2^{*2} - R_1^{*2}} \frac{I}{V_e} + \frac{C}{R_2^{*2} - R_1^{*2}} \left(\frac{\partial A_1}{\partial L_e^*} F_1 + \frac{\partial B_1}{\partial L_e^*} F_2 + R_2^* \langle c_A^* \rangle^f \big|_{R_2^*} \right) \tag{21}$$

As a result, the optimal electrode thickness can be estimated analytically once the electrode features are provided, namely ℓ_R, a_v^*, D_{eff}^* and R_1^*. Once these porous medium properties are fixed, the value of L_e^{*op} can be computed as it only depends on the conditions at which it is supposed to operate, *i.e.*, *Ki* and L_N^*. In the case of the FCC structure considered so far, and with the parameters reported in Table 1, together with $L_e^{*0} = 1$, L_e^{*op} was computed from Eq. 20 for *Ki* values up to 2×10^{-3}. The corresponding results are reported in Figure 9(a) considering two values of the diffusion layer thickness, namely $L_N = 100\ \mu$m and $L_N = 200\ \mu$m. As expected, L_e^{*op} increases when L_N decreases. This is due to the fact that a thinner diffusion layer (*i.e.* imposing a Dirichlet boundary condition closer to the fluid porous layer interface) allows a more efficient penetration of the reagent inside the porous electrode so that a thicker active layer is permitted. In addition, the optimal thickness obtained with the hybrid model reported elsewhere[17] is also represented in this figure.

As can be observed on this figure, the difference between the predictions of the two models remains very small. This is highlighted in Figure 9(b) representing the relative error between the two predictions, taking the Bessel's solution as the reference. Indeed, the largest difference is for the smallest values of *Ki* (*i.e.* for the largest values of *E*) and small values of the diffusion layer thickness. For the case under study, this difference does not exceed 6%.

These results show that the hybrid model remains robust if one is willing to estimate the optimal thickness of the electrode although it can significantly underestimate the current, in particular for the smallest values of the potential when the condition $2L_e^*/(R_1^* + R_2^*) \ll 1$ is not satisfied.

The normalized optimal thickness predicted for the other microstructures (C and BCC), compared to the FCC structure, is represented in Figure 10. Clearly, the dependence of L_e^{*op} on *Ki* is similar whatever the structure. This brings to the general conclusion that, whatever the microstructure, the optimal thickness decreases rapidly with the kinetic number and tends to a constant value for large values of *Ki.* Quantitatively, the comparison of the optimal thickness of the three structures must be made with care as L_e^{*op} and *Ki* are based on ℓ_R which is not the same from one structure to another. For this purpose, a representation where $\ell_p = d_s$ (identical for C, BCC and FCC) is used as the reference length is given in the inset of Figure 10. It

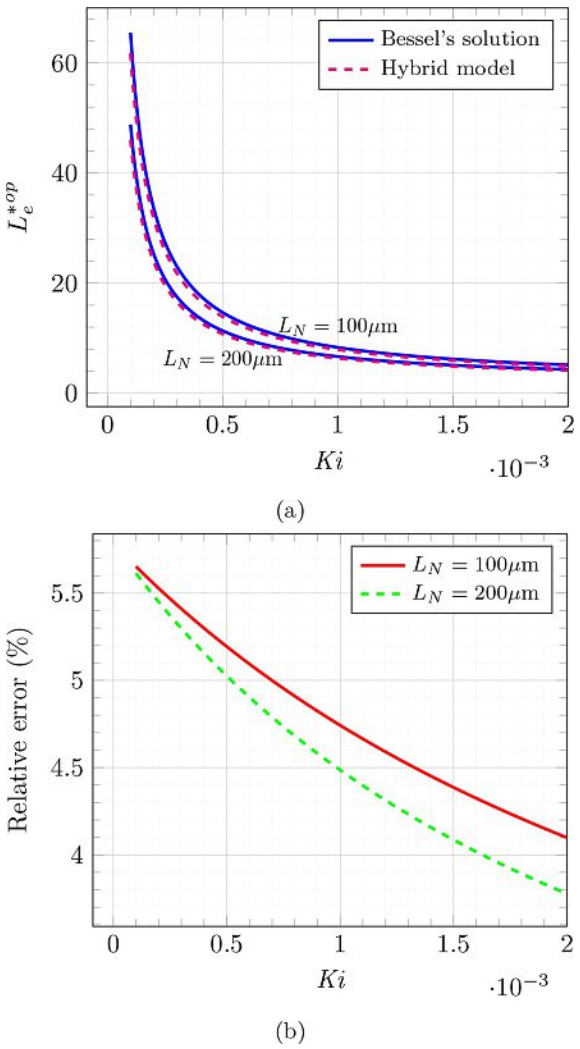

Figure 9. (a) Optimal thickness versus the kinetic number for two values of the diffusion layer thickness, obtained from the Bessel's solution and hybrid model (b) Absolute relative error between the two approaches taking the values obtained with the Bessel's solution as the reference. FCC structure. Parameters are those reported in Table 1.

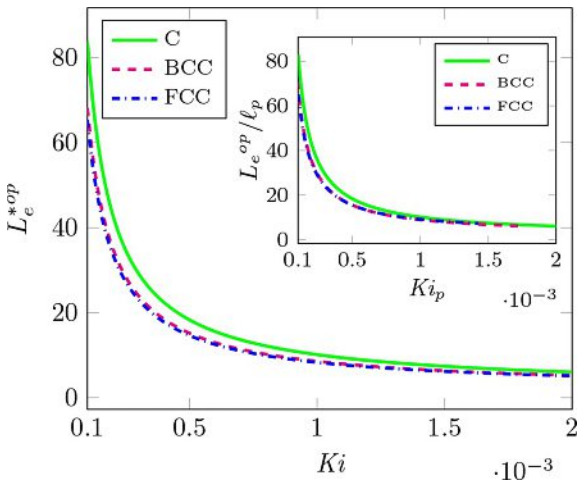

Figure 10. Optimal thickness versus the kinetic number for C, BCC and FCC structures. $L_N = 100\ \mu$m. For all structures, d_c and d_s are the same (see Table 1) featuring different values of ε, a_v, D_{eff}^* and ℓ_R (see the values in Table 1 for the FCC and in Table 2 for the C and BCC structures respectively). All other parameters are the same and are reported in Table 1. Inset: L_e^{op} made dimensionless by the spherical pore diameter, $\ell_P = d_s$, versus the pore kinetic number, $Ki_p = \frac{k_0 a_v \ell_p}{D_A}$ for the three structures.

shows that the optimal thickness for the BCC and FCC structures is almost the same (it is slightly larger for the former), but is larger for the C structure. The physical explanation of this behavior can be deduced after examining the reduced sensibility of L_e^{*op} to a_v and D_{eff}^* that are reported in Figure 11. It should be noted that the reduced sensibility of L_e^{*op} to the parameter u is defined as $u\partial L_e^{*op}/\partial u$. This figure shows that the reduced sensibility to a_v is negative (*i.e.* L_e^{*op} increases when a_v decreases) and is much larger in magnitude than that to D_{eff}^*. Consequently, the contrast on L_e^{*op} between the three structures can be interpreted only considering a_v. Since a_v is not markedly different for the BCC and FCC structures (although slightly smaller for the former) but significantly smaller for the C structure (see Tables 1 and 2), the expected variation of L_e^{*op} with respect to the structure is exactly that observed in Figure 10 and mentioned above.

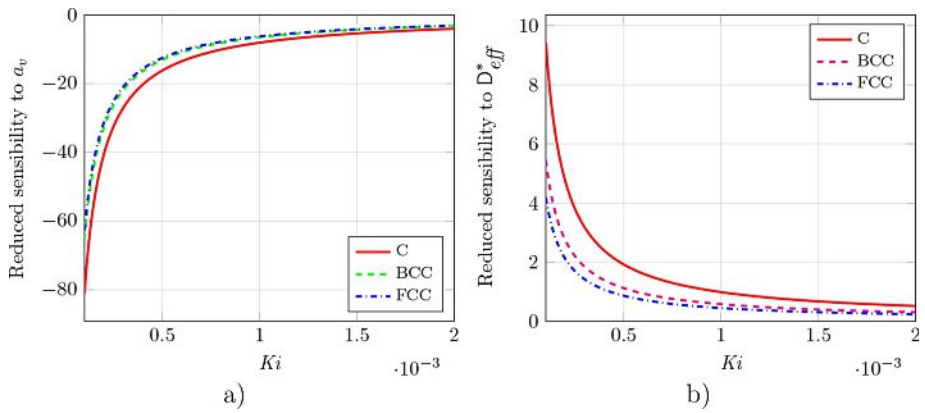

Figure 11. Reduced sensibility of L_e^{op} to a) a_v and b) D_{eff}^* for the three structures C, BCC and FCC.

Finally, it is of interest to investigate which structure, among the three considered here, is the most efficient in terms of current production. Results of the current per unit length, L, of the electrode at its optimal thickness are represented in Figure 12 for the C, BCC and FCC structures versus *Ki*. From this figure, it can be readily concluded that the FCC structure produces the largest current per unit length. In addition to the fact that it also allows the thinner optimal thickness, this structure is the most advantageous one among the three simple cases envisaged here. In what follows, results are only illustrated for a FCC structure.

4. Planar electrode

For the sake of completeness, the case of a planar electrode is now investigated by providing the analytical solution for the current and optimal thickness. In this situation, the porous material is deposited onto a plane solid surface, as in the cases envisaged by Barnes *et al.*[15] and Cai *et al.*,[26] for instance. Assuming that the extension of the electrode in both directions of the plane are much larger than the electrode thickness, the model reduces to one dimension, in the z-direction orthogonal to the plane. Using the same dimensionless variables as in section 4, the problem can be formulated as follows

$$\frac{\partial^2 \langle c_A^* \rangle^f}{\partial z^{*2}} - \varphi^2 \langle c_A^* \rangle^f = 0 \qquad 0 \le z^* \le L_e^* \tag{22a}$$

$$\frac{\partial}{\partial z^*}\left(\frac{\partial c_A^*}{\partial z^*}\right) = 0 \qquad L_e^* \le z^* \le L_e^* + L_N^* \tag{22b}$$

$$\text{B.C.1}\ \ \frac{\partial \langle c_A^* \rangle^f}{\partial z^*} = 0 \qquad z^* = 0 \tag{22c}$$

$$\text{B.C.2}\ \ \langle c_A^* \rangle^f = c_A^* \qquad z^* = L_e^* \tag{22d}$$

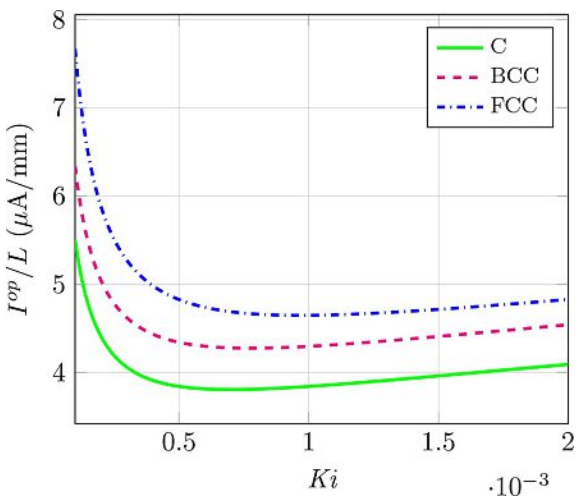

Figure 12. Current per unit length, L, of the electrode at its optimal thickness for the three structures C, BCC and FCC versus *Ki*. Parameters are those reported in Table 1.

$$\text{B.C.3}\ \ D_{eff}^* \frac{\partial \langle c_A^* \rangle^f}{\partial z^*} = \frac{\partial c_A^*}{\partial z^*} \qquad z^* = L_e^* \tag{22e}$$

$$\text{B.C.4}\ \ c_A^* = 1 \qquad z^* = L_e^* + L_N^* \tag{22f}$$

The analytical solution to the above system of equations is given by

$$\langle c_A^* \rangle^f = a_2 \cosh(\varphi z^*) \qquad 0 \le z^* \le L_e^* \tag{23a}$$

$$c_A^* = b_2 z^* + c_2 \qquad L_e^* \le z^* \le L_e^* + L_N^* \tag{23b}$$

where the coefficients a_2, b_2 and c_2 have the following expressions

$$a_2 = \left[\cosh(\varphi L_e^*) + D_{eff}^* \, \varphi L_N^* \sinh(\varphi L_e^*)\right]^{-1} \tag{24a}$$

$$b_2 = \left[\frac{\coth(\varphi L_e^*)}{D_{eff}^* \, \varphi} + L_N^*\right]^{-1} \tag{24b}$$

$$c_2 = 1 - b_2(L_e^* + L_N^*) \tag{24c}$$

Using Eq. 23a in Eq. 6, the current per unit volume, V_e, can be written as

$$I/V_e = -\frac{nFk_0\alpha_A a_v c_A^0}{\varphi L_e^* [\coth(\varphi L_e^*) + D_{eff}^* \, \varphi L_N^*]} \tag{25}$$

Its derivative with respect to L_e^* can then be expressed as

$$\frac{\partial |I/V_e|}{\partial L_e^*} = -\frac{nFk_0\alpha_A a_v c_A^0}{\varphi} \frac{\varphi(1 - \coth^2(\varphi L_e^*))L_e^* + \coth(\varphi L_e^*) + D_{eff}^* \varphi L_N^*}{[\coth(\varphi L_e^*)L_e^* + D_{eff}^* \, \varphi L_N^* L_e^*]^2} \tag{26}$$

From these two last relationships, the optimal thickness can be determined by making use of Eq. 20. The results of this prediction is represented in Figure 13 considering a FCC structure, $L_N = 100\,\mu$m $L_e^{*0} = 1$ and *Ki* up to 2×10^{-3}, all the other parameters being those reported in Table 1. As a validation, the solution of the complete model in the limit $R_1 \to \infty$ is also reported in this figure, showing that, in this limit, the two predictions perfectly match, as expected. This confirms that the complete solution is a general one, whatever the electrode dimensions.

On the basis of this general result, the analysis can be carried on to determine the optimal radius, R_1^{*op}, of the supporting wire and this is the objective of the following section.

5. Optimal wire radius, R_1^{*op}

A comparison of the results reported in Figure 13 with those in Figure 9(a) indicates that, all parameters being the same, the optimal thickness of the planar electrode is smaller than that of

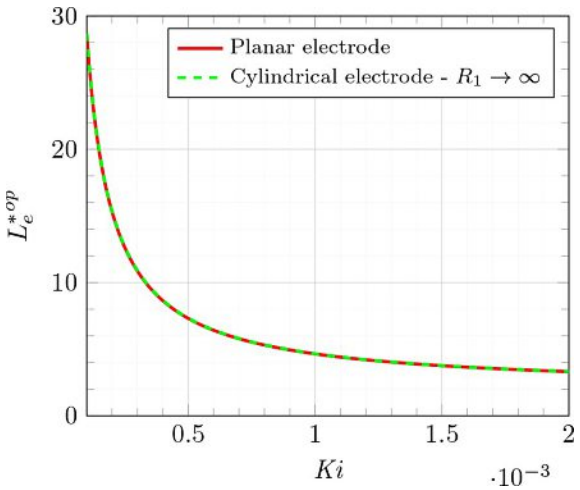

Figure 13. Optimal thickness versus the kinetic number obtained for planar electrode and cylindrical electrode taking $R_1 \to \infty$. $L_N = 100\ \mu$m. FCC structure. All the parameters are those reported in Table 1.

a cylindrical electrode having a finite radius. The contrast between the two is more significant when *Ki* decreases. This suggests to further analyze the dependence of L_e^{*op} upon the wire radius, R_1^*, for a given set of the physico-chemical parameters. More particularly, it is of interest to investigate the variation of the volume (per unit length, *L*) of the electrode at its optimal thickness, V_e^{op}/L, with respect to R_1^*. Such a variation is illustrated in Figure 14, considering two values of *Ki*, namely $Ki = 5\times10^{-4}$ and $Ki = 10^{-3}$, taking $L_N = 100\ \mu$m, all other parameters being those reported in Table 1 and a FCC structure.

This figure clearly shows that V_e^{op}/L exhibits a minimum which means that there exists a particular value of R_1^*, denoted R_1^{*op}, which minimizes the volume of material necessary to achieve the optimal thickness. This is extremely important keeping in mind that the porous medium is usually made of expensive materials using complex procedures. In Figure 15, R_1^{*op} is represented versus *Ki* in the range $10^{-4} \leq Ki \leq 10^{-3}$ for $L_N = 100\ \mu$m. As can be seen on this graph, the optimal wire radius decreases when *Ki* increases. Moreover, R_1^{*op} seems to very weakly depend on L_N, as indicated by Figure 16 where R_1^{*op} is represented versus L_N ranging from 100 μm to 400 μm for $Ki = 5\times10^{-4}$ and $Ki = 10^{-3}$.

This suggests that the value of R_1^{*op} can be determined regardless of the value of L_N, *i.e.* as only a function of *Ki* when the microstructural parameters are fixed.

This last analysis completes the optimization procedure of the electrode macroscopic dimensions as its thickness and supporting wire diameter can be predicted in order to obtain the optimal current per unit volume when the operating conditions and the microstructure of the porous material are known. This represents a major result of this work.

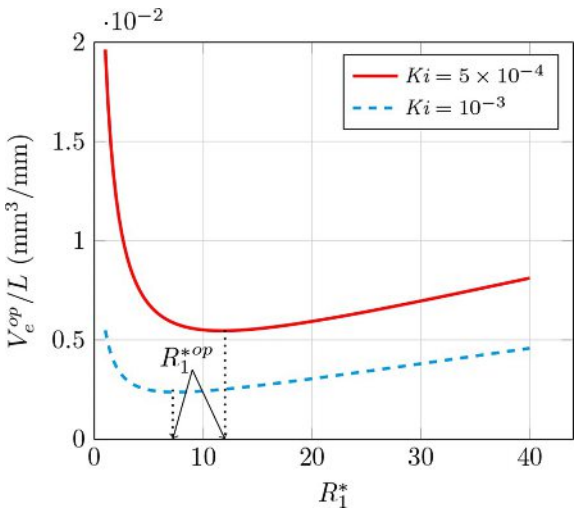

Figure 14. Variation of the volume (per unit length, *L*) of the electrode at its optimal thickness, V_e^{op}/L, versus the dimensionless wire radius, R_1^*, for $Ki = 5\times10^{-4}$ and $Ki = 10^{-3}$, taking $L_N = 100\ \mu$m (see Table 1 for the other parameters). FCC structure.

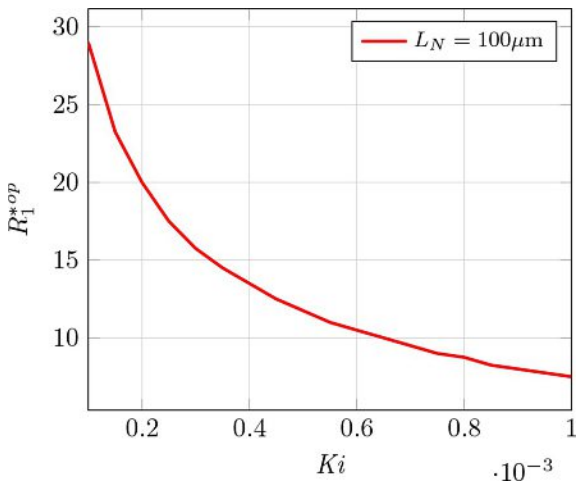

Figure 15. Variation of the dimensionless optimal wire radius, R_1^{*op}, versus *Ki* for $L_N = 100\ \mu$m (see Table 1 for the other parameters). FCC structure.

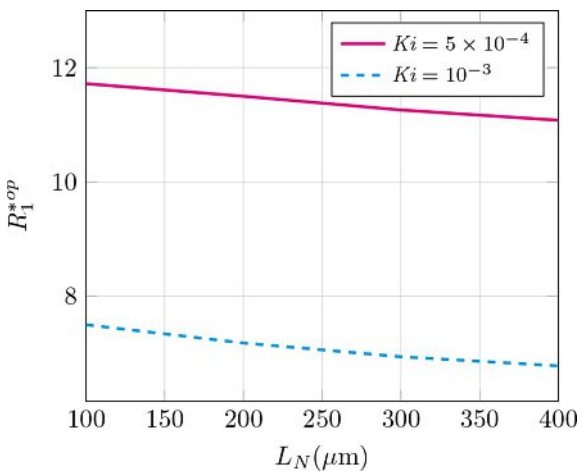

Figure 16. Variation of the dimensionless optimal wire radius, R_1^{*op}, versus L_N for $Ki = 5\times10^{-4}$ and $Ki = 10^{-3}$ (see Table 1 for the other parameters). FCC structure.

6. Conclusion

In this work, steady-state solutions of the macroscopic model describing the coupled process of electrochemical heterogeneous reaction and diffusion are developed for cylindrical and planar porous micro-electrodes.

The complete solution developed here provides a more accurate prediction of the current delivered by the electrode versus the applied potential than the hybrid model reported earlier which is recovered in the limit of a thickness to inner radius ratio much smaller than unity and which remains valid in this limit. Moreover, the complete solution also matches the one developed in the case of a planar electrode in the limit of exceedingly large radii. This makes the complete solution a general one, whatever the dimensions and microsctructure of the electrode, the characteristics of the latter being reflected in the porosity, specific area and effective diffusion coefficient. The use of this complete solution is strongly recommended particularly when the constraint on the dimensions is not satisfied.

More importantly, it is shown that an optimal radius of the supporting wire exists for a given set of the physico-chemical parameters defining the operating conditions of the electrode. This optimal radius is derived as to satisfy the minimum volume of the porous material required to ensure the optimal current per unit volume. This represents a salient result of the present work.

Together with the prediction of the current delivered by the electrode, the solution derived here allows for the determination of the electrode optimal dimensions in terms of its thickness and inner radius. This provides a complete and effective operational procedure of optimization of the macroscopic characteristics of cylindrical electrodes operating a single reduction reaction as a predictive tool for their practical design. As a final remark, it should be noticed that the approach developed here may be advantageously employed for the optimal design of other electrochemical devices devoted to energy production which architecture and operating conditions share similarities with those envisaged in this work.

Acknowledgment

This work was supported by the ANR project MOMA (ANR-17-CE08-0005).

Keywords: Porous micro-electrode · Optimal thickness · Optimal radius · Analytical solution · Volume averaging method

[1] A. Zebda, J. Alcaraz, P. Vadgama, S. Shleev, S. D. Minteer, F. Boucher, P. Cinquin, D. K. Martin, *Bioelectrochemistry* **2018**, *124*, 57–72.
[2] A. Walcarius, A. Kuhn, *TrAC Trends Anal. Chem.* **2008**, *27*, 593–603.
[3] D. Leech, P. Kavanagh, W. Schuhmann, *Electrochim. Acta* **2012**, *84*, 223–234.
[4] S. Cosnier, A. J. Gross, A. L. Goff, M. Holzinger, *J. Power Sources* **2016**, *325*, 252–263.
[5] S. Shleev, *ChemPlusChem* **2017**, *82*, 522–539.
[6] M. Gamella, A. Koushanpour, E. Katz, *Bioelectrochemistry* **2018**, *119*, 33–42.
[7] T. D. Le, D. Lasseux, X. P. Nguyen, G. L. Vignoles, N. Mano, A. Kuhn, *Chem. Eng. Sci.* **2017**, *173*, 153–167.
[8] T. D. Le, L. Zhang, A. Kuhn, N. Mano, G. L. Vignoles, D. Lasseux, *J. Electroanal. Chem.* **2019**, *855*, 113325.
[9] T. Q. N. Do, M. Varničić, R. Hanke-Rauschenbach, T. Vidaković-Koch, K. Sundmacher, *Electrochim. Acta* **2014**, *137*, 616–626.
[10] T. Q. N. Do, M. Varničić, R. Flassig, T. Vidaković-Koch, K. Sundmacher, *Bioelectrochemistry* **2015**, *106*, 3–13.
[11] S. Reculusa, M. Heim, F. Gao, N. Mano, S. Ravaine, A. Kuhn, *Adv. Funct. Mater.* **2011**, *21*, 691–698.
[12] A. Karajić, S. Reculusa, M. Heim, P. Garrigue, S. Ravaine, N. Mano, A. Kuhn, *Adv. Mater. Interfaces* **2015**, *2*, 1500192..
[13] R. D. Levie, *Adv. Electrochem. Electrochem. Eng.* **1967**, *6*, 329–397.
[14] O. E. Barcia, E. D'Elia, I. Frateur, O. R. Mattos, N. Pebere, B. Tribollet, *Electrochim. Acta* **2002**, *47*, 2109–2116.
[15] E. O. Barnes, X. Chen, P. Li, R. G. Compton, *J. Electroanal. Chem.* **2014**, *720–721*, 92–100.
[16] D. Zhang, A. Bertei, F. Tariq, N. Brandon, Q. Cai, *Prog. Energy* **2019**, *1*, 012003, 2019.
[17] T. D. Le, L. Zhang, G. L. Vignoles, N. Mano, A. Kuhn, D. Lasseux, *ChemElectroChem* **2019**, *6*, 173–180.
[18] A. Fick, *J. Membr. Sci.* **1995**, *100*, 33–38.
[19] S. Whitaker, *Rev. Mex. Ing. Quim.* **2009**, *8*, 213–243.
[20] J. A. V. Butler, *Trans. Faraday Soc.* **1924**, *19*, 729–733.
[21] S. Whitaker, *The Method of Volume Averaging.* Dordrecht, The Netherlands: Kluwer Academic Publishers, 1999.
[22] J. C. Slattery, *Advanced Transport Phenomena* (Cambridge Series in Chemical Engineering). Cambridge University Press, 1999.
[23] F. Howes, S. Whitaker, *Chem. Eng. Sci.* **1985**, *40*, 1387–1392.
[24] W. Gray, *Chem. Eng. Sci.* **1975**, *30*, 229–233.
[25] A. D. Polyanin, V. F. Zaitsev, *Handbook of Exact Solutions for Ordinary Differential Equations.* Chapman and Hall/CRC, 3rd Ed., **2003**.
[26] Q. Cai, C. S. Adjiman, N. P. Brandon, *Electrochim. Acta* **2011**, *56*, 10809–10819.